Diagnosing the fast-heating process of the double-cone ignition scheme with x-ray spectroscopy

Yu Dai [1,2], Haochen Gu [1,2], Ke Fang [1], Yihang Zhang [1], Chenglong Zhang [1,3], Yufeng Dong [1], Zhe Zhang [1,4,5], Xiaohui Yuan [6,4], Yutong Li [1,2,4,5] and Jie Zhang [1,4,6]

[1] *Beijing National Laboratory for Condensed Matter Physics, Institute of Physics, Chinese Academy of Sciences, Beijing, China*

[2] *School of Physical Sciences, University of Chinese Academy of Sciences, Beijing, China*

[3] *Department of Physics, College of Science, China University of Mining and Technology, Beijing, China*

[4] *Collaborative Innovation Center of IFSA, Shanghai Jiao Tong University, Shanghai, China*

[5] *Songshan Lake Materials Laboratory, Dongguan, China*

[6] *Key Laboratory for Laser Plasma (MOE) and School of Physics and Astronomy, Shanghai Jiao Tong University, Shanghai, China*

Correspondence to: Zhe Zhang, Beijing National Laboratory for Condensed Matter Physics, Institute of Physics, Chinese Academy of Sciences, Beijing 100190, China. Email: zzhang@iphy.ac.cn; Jie Zhang, Key Laboratory for Laser Plasma (MOE) and School of Physics and Astronomy, Shanghai Jiao Tong University, Shanghai 200240, China. Email: jzhang1@sjtu.edu.cn

Abstract: In the double-cone ignition scheme of inertial confinement fusion, the head-on collision of two compressed fuel jets from the cone-tips forms an isochoric plasma, which is then heated suddenly by an MeV relativistic electron beam produced by ultra-intense picosecond laser pulses. This fast-heating process was studied experimentally at the Shenguang II upgrade laser facility. By observing temporal resolved x-ray emission and spatial resolved x-ray spectrum, the colliding process and heating process are carefully

This peer-reviewed article has been accepted for publication but not yet copyedited or typeset, and so may be subject to change during the production process. The article is considered published and may be cited using its DOI.

10.1017/hpl.2024.32

studied. The colliding plasma was imaged to have dimensions of ~86 μm in the implosion direction and ~120 μm in the heating direction. By comparing the simulated plasma x-ray spectrum with experimental data, the electron temperature of the heated plasma was found to rapidly increase to 600±50 eV, almost doubled temperature achieved before the heating laser incidence.

Key words: fast ignition, plasma spectroscopy, direct drive, inertial confinement fusion

I. INTRODUCTION

Scientific feasibility of the inertial confinement fusion has been demonstrated by the first success of the deuterium-tritium (DT) fusion ignition at the National Ignition Facility (NIF) in December 2022 [1, 2]. However, the coupled compression and heating processes in the central ignition scheme leads to instabilities of compression and low heating efficiency. Fast ignition was proposed as an alternative approach for high-gain laser fusion because it decouples the fuel compression from fuel ignition, leading to a more stable compression and efficient ignition [3].

In the fast ignition scheme, ultra-intense laser pulses are utilized to generate a relativistic electron beam (REB), injecting into the pre-compressed isochoric plasma. The REB then travels forward as a strong current, heating the high-density fuel to generated a hot spot [4-8]. Research conducted over the past few decades has demonstrated that a guiding cone for heating could enhance efficiency by reducing the distance from the source to the core. This method has shown promising results in experiments and holds potential for further advancements in the field of fast ignition[8-12]. However, generating isochoric high-density plasmas with sharp ends has been challenging.

https://doi.org/10.1017/hpl.2024.32 Published online by Cambridge University Press

One emerging solution comes with the double cone ignition (DCI) scheme[13]. The DCI employs focused nanosecond laser beams to implode the DT fuels embedded in two head-on gold cones; collision of compressed plasma jets from tips of the cones forms an isochoric plasma with sharp ends so that the high-current REB in 10 ps, guided by a kilo-Tesla magnetic field[14], may be efficiently injected into the compressed fuel to trigger ignition suddenly. Positioned between the main cones is a heating cone, with its closed end directed towards the collision point at a distance of tens of micrometers. An ultra-intense laser pulse is then directed into the heating cone to generate energetic electrons that heat the fuel. Previous experiments have successfully validated the first three steps of the DCI scheme[15]. Eight compressing laser beams with a total energy of 14 kJ were used to drive chlorine-doped polystyrene shells ($C_{16}H_{14}Cl_2$, CHCl), resulting in a colliding plasma with a central density of up to a few g/cm^3, an areal density of 100 mg/cm^2, and a confinement time of 200 ps. The head-on collision effectively enhances the density of the plasma by several times, preheats the fuel, and efficiently converts kinetic energy into internal energy.

The DCI scheme allows for a relatively low implosion velocity, resulting in only 20%-30% of the internal energy of the fuel being obtained from the compressing lasers, with the remaining 70%-80% required from the heating lasers [10]. Therefore, fast heating plays a crucial role in the DCI scheme. In this study, we have conducted an experiment to investigate the fast-heating effect in DCI on Shenguang II upgrade laser facility (SG-II UP). Through the analysis of time-resolved x-ray images and spatial-resolved spectra, it is confirmed that the high-density collisional plasma is significantly heated by the heating laser beam. The observation of 2.7-2.8 keV Cl K-emission lines from the collisional plasma allows for temperature estimate by comparing the calculated emission spectrum using a collisional-radiative code. The analysis reveals that the implosion core is heated to 600±50 eV, nearly twice the temperature achieved before fast-heating.

https://doi.org/10.1017/hpl.2024.32 Published online by Cambridge University Press

II. EXPERIMENT

The experiment was performed on the SG-II UP in Shanghai Institute of Optics and Fine Mechanics, Chinese Academy of Sciences. As shown in Fig. 1(a), 8 compressing lasers @0.351 μm and 1 heating laser @1.05 μm were employed to compress and heat the fuel respectively. The total energy of the compressing lasers was 14 kJ with 4.7 ns duration. For uniform irradiation, continuous phase plates (CPP) were used to smooth the compressing beams resulting in a ϕ=700 μm focusing spot for every single beam. The waveform of compressing lasers shown in Fig. 1(b) was designed by Multi-1D code [16], and has been optimized with artificial intelligence algorithm to achieve a quasi-isentropically compression [17]. Simulated results from Multi-1D accorded quite well with the experimental results on the shell velocity of the plasma jets ejected from the vertex. Two spherical shells placed in the main cones were compressed and accelerated towards to the geometric center by directly driving and finally collide together at the center of the two cones. The material of the shells was chlorine-doped polystyrene in which Cl is at 6% atomic ratio. When the areal density of the colliding plasma comes to the maximum, the heating laser beam of 500 J with 10 ps duration was injected on a golden planar target assembled between the two cones to produce fast electrons. The incident angle is 9° from the normal of the golden plane. Heating cone was replaced by a golden plane here to reduce the difficulty in assembling and aiming. The focal spot of the heating laser was 30 μm in diameter, which leads to an $I\lambda^2=7.7\times10^{18}$ W·μm^2·cm^{-2}. The thickness of the golden plane was 20 μm and its rear surface is 46 μm from the colliding center.

As for diagnosis, an x-ray Kirkpatrick-Baez (KB) microscope coupled with a framing camera was installed on the equator nearly perpendicular to the heating laser to monitor the time-resolved self-emission of the colliding plasma. Its spatial and temporal resolution were ~10 μm

https://doi.org/10.1017/hpl.2024.32 Published online by Cambridge University Press

and 90 ps. The camera was response to x-ray from 1.0 keV to 3.5 keV by installing a 25 μm beryllium filter [18].

A spatial resolved flat crystal spectrometer was also placed on the equator to diagnose the x-ray spectrum. Its field view was large enough to observe the colliding and the coronal area. It was set on the rear side of the golden plane at 45° from the normal direction to avoided the interference of the self-emission produced by the heating laser or visual obstruction by target holder. A potassium acid phthalate (KAP) crystal (2d=26.7 Å) was positioned at 181 cm from the target chamber center (TCC). SR-type image plate [19] was placed 20 cm from the crystal. At the entrance of the spectrometer, a transverse slit of 10 μm width and 5 mm length was utilized to realize a spatial resolution in the vertical direction. Its spatial resolution is 19.1 μm which is high enough to distinguish the x-ray from corona and colliding region. The Bragg angle was set to 9.7°, encompassing a measuring range from 2.66 keV to 2.85 keV. This range covers the He_α line and the associated satellite lines originating from Cl^{15+} and Cl^{14+}. In order to maintain good contrast, distinct filter configurations were implemented at various height inside the spectrometer so that faint signals from colliding area can be detected without any saturation caused by coronal emission. Consequently, the ultimate transmittance was approximately 2% for the corona and 89% for the colliding area.

III. EXPERIMENTAL RESULTS

Time-resolved 2D images of the colliding plasmas measured by the KB camera are shown in Fig. 2. Images (a) to (d) show a shot without heating. Images (e) to (h) show a shot with heating. Image (i) is a schematic geometrical configuration of the image (f) marking with the targets and the heating laser beam. When the plasmas collide together, the forward kinetic energy is transferred

https://doi.org/10.1017/hpl.2024.32 Published online by Cambridge University Press

to the internal energy by strong coulomb interaction. The electron temperature increases to 340~390 eV due to the collisional preheat [18]. The bright spots in images (a) to (d) refer to the emission from the colliding plasma. In images (e) to (h), the other spots arisen on the left are caused by the heating beam. The colliding plasma in image (b) is ~86(± 6) μm high and ~120(± 6) μm (normalized intensity above 50%, and the errors come from the KB mirrors and the framing camera together[18]) without heating. When the heating laser beam is injected at 6.30(± 0.08) ns, x-rays caused by the heating beam arises and reaches its maximum at 6.46(± 0.08) ns. The luminous region caused by the heating laser pulse is shaped by the main cones and the golden plane. As can be seen in image (i), its central area is aligned with the colliding plasma indicating good directivity of the heating laser beam. Under the injection of the heating beam, a transverse high-temperature channel (normalized intensity above 50%) is formed with a length of 134 μm and a height of 53 μm. Compared to the colliding plasma, the self-emission is enhanced by 30% with the heating laser pulse. While, the stagnated duration is approximately invariant.

Figure 3(a) shows the space-resolved spectrum from 2.70-2.85 keV obtained by the crystal spectrometer. The transverse slit gives the spatial resolution in vertical direction so that the spectrum can be divided into three regions. The spectrum at the top and the bottom comes from the coronal plasma directly heated by the compressing laser pulses. Between them is the collision area, marked with the red dashed box. The observed spectrum comprises continuous bremsstrahlung emission and line emission of Cl. The line emission consists of a resonance line ("w" at $2789.7eV$, $1s2p\,^1P_1 \rightarrow 1s^2\,^1S_0$), an intercombination line ("y" at $2775.0\,eV$, $1s2p\,^3P_1 \rightarrow 1s^2\ ^1S_0$) and a set of Li-like satellite lines ("jkl" and other small peaks) [20]. Owing to the high energy resolution of E/ΔE=1000, the spectroscopic analysis reveals three discrete peaks in the coronal and collision regions. As can be seen in Fig. 3(b), emission from the colliding region is

https://doi.org/10.1017/hpl.2024.32 Published online by Cambridge University Press

distinctly enhanced with the injected picosecond heating laser pulse. Since single cell model that assumes the plasma is uniform failed to match the experimental result, radiation-hydrodynamic simulations have been implemented to get the spatially distributed temperature and density to deduce the temperature by x-ray spectroscopy. This will be discussed in the next section. It is worth noting that relative central wavelength shifts are observed between the coronal and collision regions. Specifically, the resonance line (w) exhibited a shift of 4.0 eV, while the intercombination line (y) and the satellite lines (jkl) displayed shifts of 2.5eV and 2.0eV, respectively.

IV. DISCUSSIONS

The enhanced x-ray emission indicates that colliding plasma is heated by the REB generated by the ultra-intense laser pulses. However, simple collision-radiative codes failed to reproduce the measured spectrum. Single cell model assuming a uniform temperature and density distribution is no longer suitable for the colliding plasma. Non-local radiation field becomes important in the calculation due to the high density and the relatively soft x-ray emission. To calculate the spectrum in detail, radiation-hydrodynamics simulation and scaling theory of fast electrons are used to reproduce the experimental results. Noting that the opacity and equation of state tables used in following simulations are calculated by the PROPACEOS code.[21, 22]

Process from compression to head-on collision without the fast-heating are simulated by the FLASH ,[23] an open source radiation-hydrodynamics program. This part is simulated in two-dimensional cylindrical coordinates. Figure 4 shows the simulated results of FLASH at 2.0 ns and 6.3 ns respectively. In the first 2 ns, the CHCl shell experiences quasi-isentropic compression driven by the three pickets of compressing lasers. Subsequently, shock wave penetrates the shell, marking the onset of the acceleration phase. Hydrodynamics instabilities grow at the ablation front

https://doi.org/10.1017/hpl.2024.32 Published online by Cambridge University Press

leading to density decline. Still and all, with spherical compression and the confinement of the main cone, the density grows to 3 g/cm^3 when the fuel is pushed to the apex of the cone. Upon the collision of the two fuel segments, the forward kinetic energy was efficiently converted into internal energy, primarily facilitated by the strong coulomb collisions. Figure 5(a) and (b) show the density and temperature evolution of the shell indetial. In Fig. 5(c), the transverse distribution of the colliding plasma is presented, as obtained from numerical simulations and experimental density measurements. Experimental density measurements were conducted using monochrome backlight photography combined with Abel inversion [15]. The simulated results agree well with the experiment in terms of collision time and plasma density distribution.

As for the fast-heating process, the energy deposition of relativistic electrons was evaluated by following equation [24, 25]:

$$-\frac{\mathrm{d}E}{\mathrm{d}x}=\frac{2\pi n_e e^4}{m_e\beta^2c^2}\left[\ln\left(\frac{m_e^2c^2(\gamma-1)\lambda_D^2}{2\hbar^2}\right)+\frac{1}{8}\left(\frac{\gamma-1}{\gamma}\right)^2-\frac{2\gamma-1}{\gamma^2}\right.$$

$$\left.+1-\ln 2+\ln\left(\frac{u}{\omega_p\lambda_D}\left(\frac{2}{3}\right)^{1/2}\right)^2\right], \tag{1}$$

where u and n_e are the velocity and the electron density, $\beta=u/c$, $\gamma=(1-u^2/c^2)^{-1/2}$ is the Lorentz parameter, λ_D and ω_p are the Debye length and the plasma frequency of the colliding plasma, respectively. The considered region is within $600\,\mu m$, where the density is above 1×10^{-5}g/cm^3 and absorbs the majority of the deposited energy. According to the scaling relation, the temperature of the fast electrons is set to be 1 MeV [26, 27] which is consistent with the experimental results obtained by an image plates (IP) stack [results to be published]. Figure 5(c) shows an example of the temperature distribution before and after fast-heating. Note that the heating effects of this calculation mainly provide the profile of the temperature distribution,

https://doi.org/10.1017/hpl.2024.32 Published online by Cambridge University Press

serving as a reference input for spectral calculations. The final temperature of the stagnated plasma is derived by matching the spectral results.

Plasma spectroscopy has long been used to diagnose plasma parameters [28-31]. To aid in the qualitative assessment of experiments, plasma models and spectral simulation procedures are often employed. In this context, the SPECT3D [32], a radiation-transport atomic-kinetic codes based on a highly detailed atomic mode, is used to calculate the K-shell emission from the plasma. Since collisional depopulation affects the population distributions as well as radiation under such condition, collisional-radiative (CR) model is chosen to solve the level populations. Self-consistent coupling with radiation is dealt with multi-angle long characteristic model which computes photon-induced rates by performing radiative transfer along multiple rays that extend through the entire plasma grid. The spectral simulated results are illustrated in Fig. 6(a) with experimental data. As the intensity of "w" and "jkl" represents the population of He-like ions and Li-like ions, its ratio is commonly used to characterize the plasma temperature when the degree of ionization of the element varies monotonically over the concerned temperature range [28, 30]. Figure 6(b) gives the variation of ionization degree of Cl with temperature for different electron densities. The ratio of population and line intensity varies monotonically in concerned parameter scale. Hence, it can be concluded that the temperature of the colliding plasma has increased to approximately $600\ (\pm 50)\ \mathrm{eV}$ due to the heating effect induced by fast electrons.

Furthermore, a pronounced blue shift is evident in Fig. 6(a). For "w" and "y", two relatively isolated emission peaks, their peaks shift 4.0eV and 2.5eV respectively. In the case of "jkl" composed of a cluster of satellite lines, the shift of 2.0eV is determined by analyzing the profile involving the rising and falling edges. This phenomenon is the Doppler effect caused by the transverse diffusion of the colliding plasma. The emission peaks emerge from distinct regions of

https://doi.org/10.1017/hpl.2024.32 Published online by Cambridge University Press

the plasma, each characterized by different diffusion velocities, giving rise to these varying shifts. Figure 7(a) provides insight into the transverse velocity of the plasma, with the right y-axis indicating the Doppler shifts in eV. In Fig. 7(b), the spatial emissivity of each emission peak is presented, with each normalized by its own intensity in spatial position, ensuring that the integral of each line is 100%. This not only explains the energy shift, but also explains the broadening of the resonance line ("w") to a certain extent. According to the spatial emissivity of Fig 7(b) the spatial size of line "w" is 450 μm in radius. Its diameter is 900 μm leading to 8.03 eV broadening accounting for the main part of the broadening compared to the doppler broadening of 0.88 eV and instrumental broadening of 0.48 eV. In addition, the spectral results lack temporal resolution, it is reasonable to infer that the resonance line ("w") is emitted over a larger spatial region and for a longer duration, resulting in a significantly greater broadening compared to the intercombination line ("y").

V. CONCLUSIONS

In summary, the experiment has been conducted at the SG-II UP to investigate the fast-heating of an ultra-intense petawatt laser beam in the DCI scheme. After injecting the heating beam, a substantial increase in electron temperature within the high-density stagnated plasma is achieved, leading to the excitation of tracer elements and the emission of K-shell lines. Employing radiation-hydrodynamics simulations and spectral calculations to replicate and diagnose the colliding plasma, the heated plasma temperature is estimated to be $600 \pm 50\,\mathrm{eV}$ through the comparison of experimental and simulated results. This notable heating effect is attributed to the favorable alignment between the plasma density and the temperature of the fast electrons. The observed blue

https://doi.org/10.1017/hpl.2024.32 Published online by Cambridge University Press

shift in the colliding plasma spectrum conveys useful information about its volume velocity and diffusion dynamics, providing additional insights for interpreting the spectral results.

Acknowledgements

The authors would like to thank the DCI joint team for their support of the experiment and the target fabrication. We would like to thank Dr. Yuxue Zhang from research center of laser fusion, China Academy of Engineering Physics and Dr. Feilu Wang from national astronomical observatories, Chinses Academy of Sciences for their valuable recommendations about analyzing the spectroscopy results.

This work was supported by the Strategic Priority Research Program of the Chinese Academy of Sciences (Grant Nos. XDA25010100, XDA25010300, and XDA25030100) and also in part by the National Natural Science Foundation of China (Grants No. 11827807).

Figures and tables

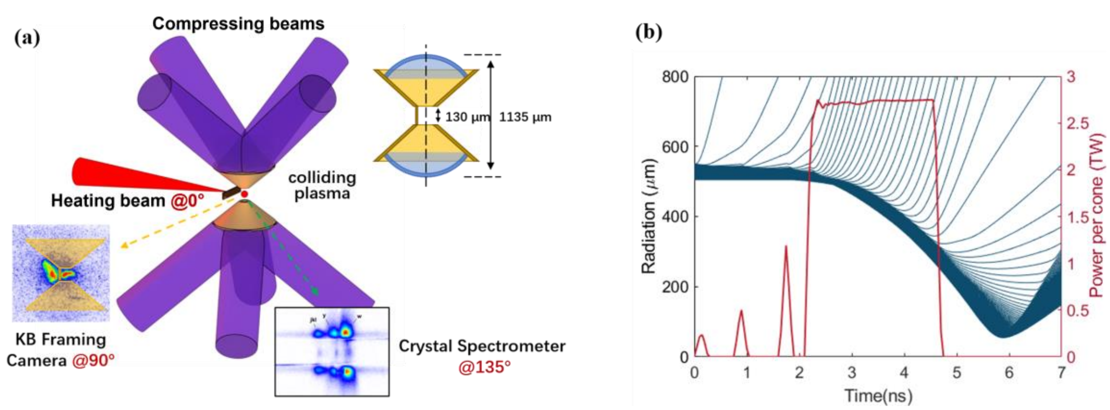

Figure 1:

https://doi.org/10.1017/hpl.2024.32 Published online by Cambridge University Press

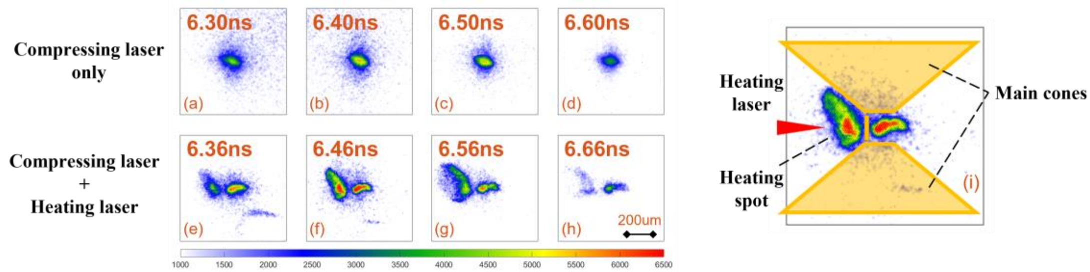

Figure 2:

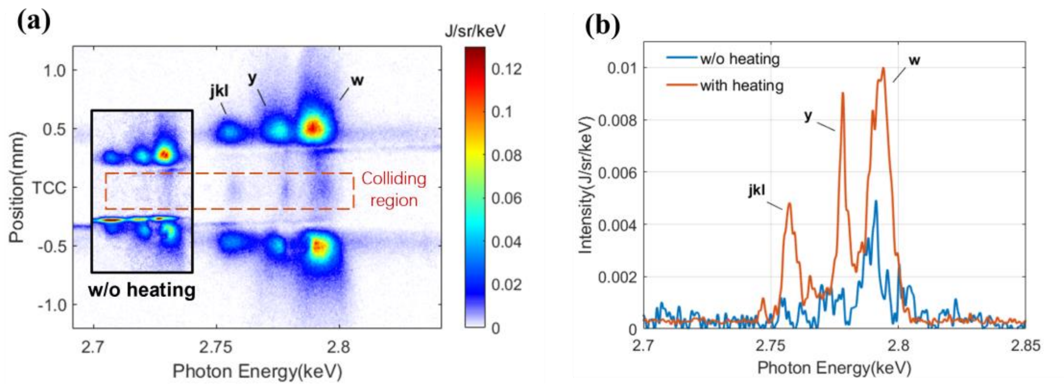

Figure 3:

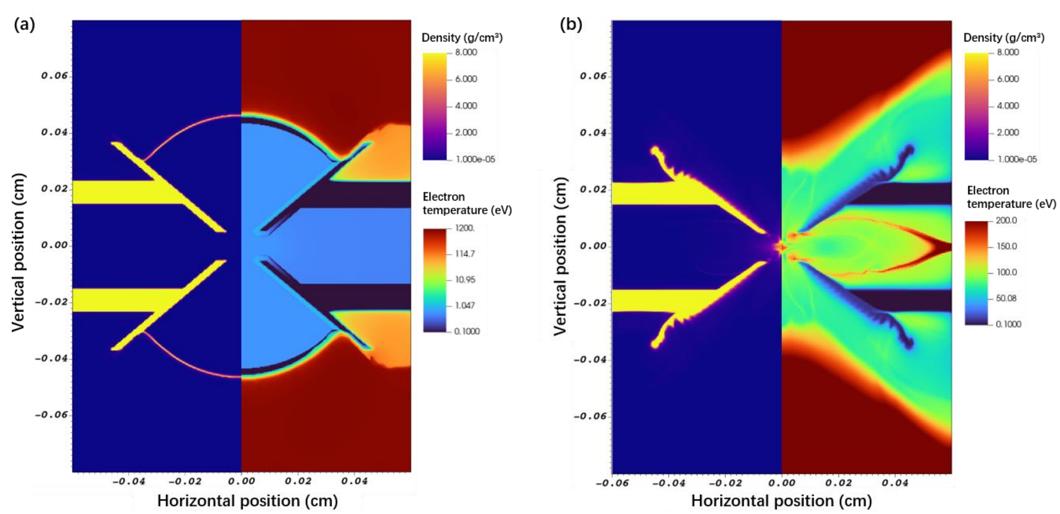

Figure 4:

https://doi.org/10.1017/hpl.2024.32 Published online by Cambridge University Press

Figure 5:
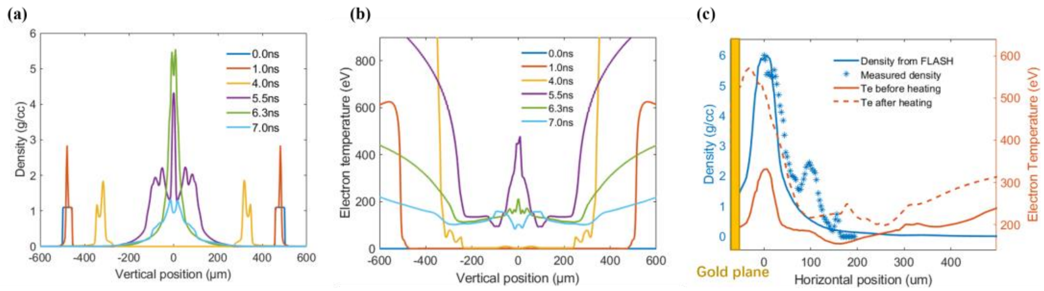

Figure 6:
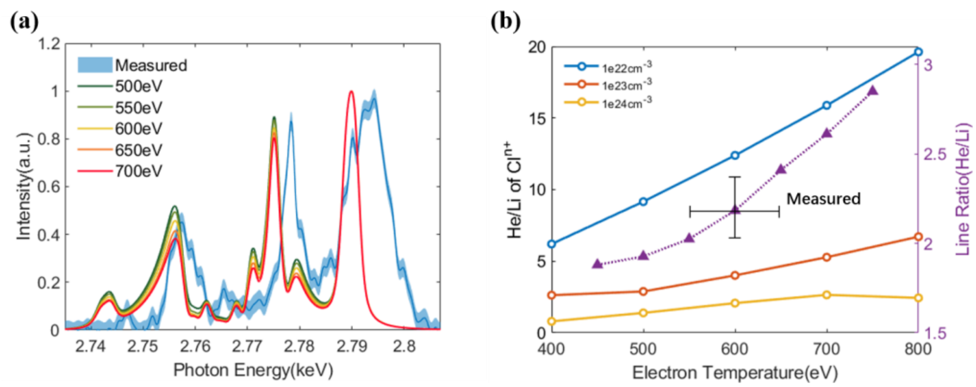

Figure 7:
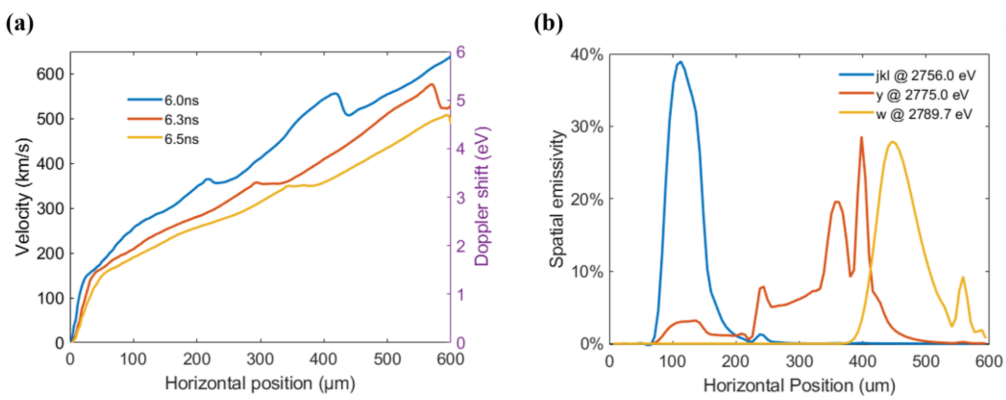

Figure captions

Figure 1: Experimental configuration and laser waveform used in the experiment. (a), 8 driving laser beams are used to directly drive the CHCl shells and push the fuel collide together at the TCC. The heating laser is injected on a golden plane placed near the TCC to generate fast electrons. (b), The laser waveform and the motion patter calculated by MULTI-1D.

https://doi.org/10.1017/hpl.2024.32 Published online by Cambridge University Press

Figure 2: The time-resolved self-emission from colliding area taken by KB framing camera. (a)-(d) are the x-ray emission of colliding plasmas without heating laser beam injected. (e)-(f) are with the heating laser beam injected from left side. The spots on the left are induced by the heating beam. (i) is (f) marked with targets and the heating laser beam.

Figure 3: (a) Spatial-resolved spectrum of shots with and without (inset) heating. (b) Profiles derived from the TCC position from the two shots (20 μm averaged on and below the TCC position), respectively.

Figure 4: The 2D simulated results of FLASH at (a) 2.0 ns and (b) 6.3 ns. The left side of them is the density distribution and the right side is the electron temperature distribution. For clarity, the color map of temperature is logarithmic in (a) and linear in (b).

Figure 5: Simulated results used to calculate the spectrum. (a) and (b) are the density and electron temperature distribution in vertical direction simulated by FLASH, respectively. (c) shows the transverse distribution of the colliding plasma. The simulated density (blue line) is compared with the experimental result (the stars). The electron temperature before (red line) and after heating (red dotted line) is also shown here.

Figure 6: (a), the comparison between the measured and the calculated spectrum. For the calculated results, temperature range from 500 eV to 700 eV is included. The measured one is the same as the Fig 3(b) "with heating" with errors marked by the shadow area. The Cl^{n+} population ratio of He-like ions to Li-like ions is shown in (b), together with the line ratio of "w" to "jkl".

Figure 7: (a), the velocity distribution of the stagnated stage derived from FLASH. (b), Spatial emissivity of the plasma in different depth along the sight line.

References

1. D. Clery, "With historic explosion, a long sought fusion breakthrough: National Ignition Facility achieves net energy “gain” with laser-powered approach" (December 13, 2022), retrieved https://www.science.org/content/article/historic-explosion-long-sought-fusion-breakthrough.
2. H. Abu-Shawareb, R. Acree, P. Adams *et al*., "Achievement of Target Gain Larger than Unity in an Inertial Fusion Experiment," Physical Review Letters **132**(2024).
3. M. Tabak, J. Hammer, M. E. Glinsky, W. L. Kruer, S. C. Wilks, J. Woodworth, E. M. Campbell, M. D. Perry, and R. J. Mason, "Ignition and high gain with ultrapowerful lasers*," Physics of Plasmas **1**, 1626-1634 (1994).
4. C. Stoeckl, T. R. Boehly, J. A. Delettrez, S. P. Hatchett, J. A. Frenje, V. Y. Glebov, C. K. Li, J. E. Miller, R. D. Petrasso, F. H. Séguin, V. A. Smalyuk, R. B. Stephens, W. Theobald, B. Yaakobi, and T. C. Sangster, "Direct-drive fuel-assembly experiments with gas-filled, cone-in-shell, fast-ignitor targets on the OMEGA Laser," Plasma Physics and Controlled Fusion **47**, B859-B867 (2005).

https://doi.org/10.1017/hpl.2024.32 Published online by Cambridge University Press

5. F. Zhang, H. B. Cai, W. M. Zhou, Z. S. Dai, L. Q. Shan, H. Xu, J. B. Chen, F. J. Ge, Q. Tang, W. S. Zhang, L. Wei, D. X. Liu, J. F. Gu, H. B. Du, B. Bi, S. Z. Wu, J. Li, F. Lu, H. Zhang, B. Zhang, M. Q. He, M. H. Yu, Z. H. Yang, W. W. Wang, H. S. Zhang, B. Cui, L. Yang, J. F. Wu, W. Qi, L. H. Cao, Z. Li, H. J. Liu, Y. M. Yang, G. L. Ren, C. Tian, Z. Q. Yuan, W. D. Zheng, L. F. Cao, C. T. Zhou, S. Y. Zou, Y. Q. Gu, K. Du, Y. K. Ding, B. H. Zhang, S. P. Zhu, W. Y. Zhang, and X. T. He, "Enhanced energy coupling for indirect-drive fast-ignition fusion targets," Nature Physics **16**, 810-814 (2020).

6. Y. Kitagawa, Y. Mori, K. Ishii, R. Hanayama, S. Okihara, Y. Arikawa, Y. Abe, E. Miura, T. Ozaki, O. Komeda, H. Suto, Y. Umetani, A. Sunahra, T. Johzaki, H. Sakagami, A. Iwamoto, Y. Sentoku, N. Nakajima, S. Sakata, K. Matsuo, R. S. Mirfayzi, J. Kawanaka, S. Fujiokua, K. Tsubakimoto, K. Shigemori, K. Yamanoi, A. Yogo, A. Nakao, M. Asano, H. Shiraga, T. Motohiro, T. Hioki, and H. Azuma, "Direct fast heating efficiency of a counter-imploded core plasma employing a laser for fast ignition experiments (LFEX)," Nuclear Fusion **62**(2022).

7. T. Ozaki, Y. Abe, Y. Arikawa, Y. Sentoku, J. Kawanaka, S. Tokita, N. Miyanaga, T. Jitsuno, Y. Nakata, K. Tsubakimoto, A. Sunahara, T. Jhozaki, E. Miura, O. Komeda, A. Iwamoto, H. Sakagami, S. Okihara, K. Ishii, R. Hanayama, Y. Mori, and Y. Kitagawa, "Hot electron and ion spectra on blow-off plasma free target in GXII-LFEX direct fast ignition experiment," Nuclear Fusion **63**(2023).

8. P. Norreys, D. Batani, S. Baton, F. N. Beg, R. Kodama, P. M. Nilson, P. Patel, F. Pérez, J. J. Santos, R. H. H. Scott, V. T. Tikhonchuk, M. Wei, and J. Zhang, "Fast electron energy transport in solid density and compressed plasma," Nuclear Fusion **54**(2014).

9. R. B. Stephens, R. A. Snavely, Y. Aglitskiy, F. Amiranoff, C. Andersen, D. Batani, S. D. Baton, T. Cowan, R. R. Freeman, T. Hall, S. P. Hatchett, J. M. Hill, M. H. Key, J. A. King, J. A. Koch, M. Koenig, A. J. MacKinnon, K. L. Lancaster, E. Martinolli, P. Norreys, E. Perelli-Cippo, M. Rabec Le Gloahec, C. Rousseaux, J. J. Santos, and F. Scianitti, "K(alpha) fluorescence measurement of relativistic electron transport in the context of fast ignition," Phys Rev E Stat Nonlin Soft Matter Phys **69**, 066414 (2004).

10. Z. M. Sheng, Y. Sentoku, K. Mima, J. Zhang, W. Yu, and J. Meyer-ter-Vehn, "Angular Distributions of Fast Electrons, Ions, and Bremsstrahlung x/γ-Rays in Intense Laser Interaction with Solid Targets," Physical Review Letters **85**, 5340-5343 (2000).

11. P. A. Norreys, R. Allott, R. J. Clarke, J. Collier, D. Neely, S. J. Rose, M. Zepf, M. Santala, A. R. Bell, K. Krushelnick, A. E. Dangor, N. C. Woolsey, R. G. Evans, H. Habara, T. Norimatsu, and R. Kodama, "Experimental studies of the advanced fast ignitor scheme," Physics of Plasmas **7**, 3721-3726 (2000).

12. R. Kodama, P. A. Norreys, K. Mima, A. E. Dangor, R. G. Evans, H. Fujita, Y. Kitagawa, K. Krushelnick, T. Miyakoshi, N. Miyanaga, T. Norimatsu, S. J. Rose, T. Shozaki, K. Shigemori, A. Sunahara, M. Tampo, K. A. Tanaka, Y. Toyama, T. Yamanaka, and M. Zepf, "Fast heating of ultrahigh-density plasma as a step towards laser fusion ignition," Nature **412**, 798-802 (2001).

13. J. Zhang, W. M. Wang, X. H. Yang, D. Wu, Y. Y. Ma, J. L. Jiao, Z. Zhang, F. Y. Wu, X. H. Yuan, Y. T. Li, and J. Q. Zhu, "Double-cone ignition scheme for inertial confinement fusion," Philos Trans A Math Phys Eng Sci **378**, 20200015 (2020).

14. W. M. Wang, P. Gibbon, Z. M. Sheng, and Y. T. Li, "Magnetically assisted fast ignition," Phys Rev Lett **114**, 015001 (2015).

15. Z. Zhang, X.-H. Yuan, Y.-H. Zhang, H. Liu, K. Fang, C.-L. Zhang, Z.-D. Liu, X. Zhao, Q.-L. Dong, G.-Y. Liu, Y. Dai, H.-C. Gu, Y.-T. Li, J. Zheng, J.-Y. Zhong, and J. Zhang, "Efficient energy transition from kinetic to internal energy in supersonic collision of high-density plasma jets from conical implosions," Acta Physica Sinica **71**(2022).
16. R. Ramis and J. Meyer-ter-Vehn, "MULTI-IFE—A one-dimensional computer code for Inertial Fusion Energy (IFE) target simulations," Computer Physics Communications **203**, 226-237 (2016).
17. F. Wu, X. Yang, Y. Ma, Q. Zhang, Z. Zhang, X. Yuan, H. Liu, Z. Liu, J. Zhong, J. Zheng, Y. Li, and J. Zhang, "Machine-learning guided optimization of laser pulses for direct-drive implosions," High Power Laser Science and Engineering **10**(2022).
18. K. Fang, Y. H. Zhang, Y. F. Dong, T. H. Zhang, Z. Zhang, X. H. Yuan, Y. T. Li, and J. Zhang, "Dynamical process in the stagnation stage of the double-cone ignition scheme," Physics of Plasmas **30**(2023).
19. Y. Dong, Z. Zhang, M. Xu, Y. Du, C. Zhang, X. Dong, Y. He, J. Tan, Y. Zhang, C. Zhu, J. Feng, L. Cheng, Y. Li, and Y. Li, "Absolute x-ray calibration of an Amersham imaging plate scanner," Rev Sci Instrum **91**, 033105 (2020).
20. A. Kramida, Ralchenko, Yu., Reader, J. and NIST ASD Team, "NIST Atomic Spectra Database (version 5.11), [Online]." (2023), retrieved https://physics.nist.gov/asd.
21. J. J. MacFarlane, I. E. Golovkin, and P. R. Woodruff, "HELIOS-CR – A 1-D radiation-magnetohydrodynamics code with inline atomic kinetics modeling," Journal of Quantitative Spectroscopy and Radiative Transfer **99**, 381-397 (2006).
22. C. Orban, M. Fatenejad, and D. Q. Lamb, "Code-to-code comparison and validation of the radiation-hydrodynamics capabilities of the FLASH code using a laboratory astrophysical jet," Physics of Plasmas **29**(2022).
23. B. Fryxell, K. Olson, P. Ricker, F. X. Timmes, M. Zingale, D. Q. Lamb, P. MacNeice, R. Rosner, J. W. Truran, and H. Tufo, "FLASH: An Adaptive Mesh Hydrodynamics Code for Modeling Astrophysical Thermonuclear Flashes," The Astrophysical Journal Supplement Series **131**, 273 (2000).
24. C. Deutsch, H. Furukawa, K. Mima, M. Murakami, and K. Nishihara, "Interaction Physics of the Fast Ignitor Concept," Physical Review Letters **77**, 2483-2486 (1996).
25. A. A. Solodov and R. Betti, "Stopping power and range of energetic electrons in dense plasmas of fast-ignition fusion targets," Physics of Plasmas **15**(2008).
26. S. C. Wilks, W. L. Kruer, M. Tabak, and A. B. Langdon, "Absorption of ultra-intense laser pulses," Physical Review Letters **69**, 1383-1386 (1992).
27. M. G. Haines, M. S. Wei, F. N. Beg, and R. B. Stephens, "Hot-Electron Temperature and Laser-Light Absorption in Fast Ignition," Physical Review Letters **102**(2009).
28. S. H. Glenzer, C. A. Back, K. G. Estabrook, B. J. MacGowan, D. S. Montgomery, R. K. Kirkwood, J. D. Moody, D. H. Munro, and G. F. Stone, "Electron temperature and density measurements in laser-produced large-scale-length gas-bag plasmas by x-ray spectroscopy," Physical Review E **55**, 927-938 (1997).
29. M. J. Rosenberg, R. Epstein, A. A. Solodov, W. Seka, J. F. Myatt, P. A. Michel, M. A. Barrios, D. B. Thorn, M. Hohenberger, J. D. Moody, and S. P. Regan, "X-ray spectroscopy of planar laser-plasma interaction experiments at the National Ignition Facility," Physics of Plasmas **26**(2019).
30. L. Gao, B. F. Kraus, K. W. Hill, M. B. Schneider, A. Christopherson, B. Bachmann, M. Bitter, P. Efthimion, N. Pablant, R. Betti, C. Thomas, D. Thorn, A. G. MacPhee, S. Khan,

https://doi.org/10.1017/hpl.2024.32 Published online by Cambridge University Press

R. Kauffman, D. Liedahl, H. Chen, D. Bradley, J. Kilkenny, B. Lahmann, E. Stambulchik, and Y. Maron, "Hot Spot Evolution Measured by High-Resolution X-Ray Spectroscopy at the National Ignition Facility," Phys Rev Lett **128**, 185002 (2022).

31. B. F. Kraus, L. Gao, W. Fox, K. W. Hill, M. Bitter, P. C. Efthimion, A. Moreau, R. Hollinger, S. Wang, H. Song, and J. J. Rocca, "Ablating Ion Velocity Distributions in Short-Pulse-Heated Solids via X-Ray Doppler Shifts," Physical Review Letters **129**(2022).

32. J. J. MacFarlane, I. E. Golovkin, P. Wang, P. R. Woodruff, and N. A. Pereyra, "SPECT3D – A multi-dimensional collisional-radiative code for generating diagnostic signatures based on hydrodynamics and PIC simulation output," High Energy Density Physics **3**, 181-190 (2007).

https://doi.org/10.1017/hpl.2024.32 Published online by Cambridge University Press